LETTER

doi:10.1038/nature11993

Natural RNA circles function as efficient microRNA sponges

Thomas B. Hansen[1], Trine I. Jensen[1], Bettina H. Clausen[2], Jesper B. Bramsen[1,3], Bente Finsen[2], Christian K. Damgaard[1] & Jørgen Kjems[1,3]

MicroRNAs (miRNAs) are important post-transcriptional regulators of gene expression that act by direct base pairing to target sites within untranslated regions of messenger RNAs[1]. Recently, miRNA activity has been shown to be affected by the presence of miRNA sponge transcripts, the so-called competing endogenous RNA in humans and target mimicry in plants[2–7]. We previously identified a highly expressed circular RNA (circRNA) in human and mouse brain[8]. Here we show that this circRNA acts as a miR-7 sponge; we term this circular transcript ciRS-7 (circular RNA sponge for miR-7). ciRS-7 contains more than 70 selectively conserved miRNA target sites, and it is highly and widely associated with Argonaute (AGO) proteins in a miR-7-dependent manner. Although the circRNA is completely resistant to miRNA-mediated target destabilization, it strongly suppresses miR-7 activity, resulting in increased levels of miR-7 targets. In the mouse brain, we observe overlapping co-expression of ciRS-7 and miR-7, particularly in neocortical and hippocampal neurons, suggesting a high degree of endogenous interaction. We further show that the testis-specific circRNA, sex-determining region Y (*Sry*)[9], serves as a miR-138 sponge, suggesting that miRNA sponge effects achieved by circRNA formation are a general phenomenon. This study serves as the first, to our knowledge, functional analysis of a naturally expressed circRNA.

To regulate mature miRNA activity, conceptual studies overexpressing miRNA target site concatamers, so-called miRNA sponges, were initially performed and shown to result in a loss of miRNA function accompanied with increased levels of endogenous targets[10]. Subsequently, endogenously expressed linear RNAs have been shown to sequester and inhibit miRNA activity in plants (target mimicry)[2] and mammals (competing endogenous RNA)[3–7]. Collectively, these data suggest that miRNA sponges are widespread regulators of miRNA activity in many eukaryotes. However, the miRNA sponges or miRNA-competing transcripts identified so far are expressed at low levels, contain a limited number of miRNA target sites, and, similar to miRNA targets, are themselves subject to miRNA-mediated destabilization[3].

We recently identified a highly expressed endogenous circular RNA (circRNA) in human and mouse brain[8], and demonstrated that the circRNA can be endonucleolytically cleaved by miR-671 in an AGO2-dependent manner; however, the function of this circRNA remained unknown. By searching for miRNA target sites in this circRNA, we identified 73 conventional seed–targets for miR-7. Plotting the target site position and nucleotide conservation, we observed that the target sites are selectively conserved compared to the adjacent regions in all eutherian mammals but not in marsupials (Fig. 1a). Although variable in size, this circRNA, ciRS-7, exists in the genome of all eutherian mammals investigated (Supplementary Fig. 1a). A computational motif analysis of human ciRS-7 using MEME[11] revealed a high prevalence of miR-7 seed–targets with additional 3′-end base pairing; however, they are mismatched at the central part of the duplex preventing miRNA-mediated endocleavage[12,13] (Supplementary Fig. 1b). The miR-671 target site exhibits near-perfect complementarity and very little variation across species (Supplementary Fig. 1c), as well as high duplex stability compared to miR-7 (Supplementary Fig. 1d). Analysis of available online AGO2 immunoprecipitation followed by high-throughput sequencing (HITS-CLIP) data from mouse brain[14] revealed a high degree of AGO2 occupancy on the mouse variant of ciRS-7, with sequence reads dispersed throughout ciRS-7, and the highest read densities covering the region with the highest 8-nucleotide target site abundance (Supplementary Fig. 2a). Importantly, HITS-CLIP reads proximal to the nonlinear splice sites support the association between AGO2 and ciRS-7 (Supplementary Fig. 2b). This confirms our previous observation showing a high expression of ciRS-7 in human and mouse brain[8] and other studies profiling brain-specific expression of miR-7 (ref. 15).

To study the effect of ciRS-7 expression on miR-7 activity, we established a vector-based system expressing the circRNA. The biogenesis of circRNAs is at present unknown; however, previous studies have shown that exons flanked by inverted repeats induce circRNA formation *in vitro* by nonlinear splicing[16], and this is thought to be essential for production of the circular *Sry* RNA[9,17]. Thus, we inserted the ciRS-7 exon along with the endogenous flanking sequence into pcDNA3 (pcDNA3-ciRS-7-ir; Fig. 1b). Subsequently, we copied part of the upstream flanking sequence and inserted it in an inverted orientation downstream (pcDNA3-ciRS-7; Fig. 1b). Transient expression of pcDNA3-ciRS-7, but not of the construct lacking the downstream inverted sequence (pcDNA3-ciRS-7-ir), resulted in the production of a circRNA species that was indistinguishable from the endogenously expressed circRNA by northern analysis (Fig. 1c) and PCR with reverse transcription (RT–PCR; Supplementary Fig. 3a). In addition, we constructed a linear and polyadenylated miR-7 sponge containing all miR-7 sponge sites but excluding the splice sites and flanking sequences (ciRS-7-fs; Fig. 1b and Supplementary Fig. 4a). Enzymatic digestion of linear RNA by tobacco acid pyrophosphatase followed by either terminator exonuclease or RNase R cleavage confirmed a circular structure of the RNA produced from ciRS-7 (Supplementary Fig. 3b, c). By co-expressing the circRNA- or the linear RNA-producing vectors with miR-7 or miR-769 expression vectors, ciRS-7 levels remained unaffected, whereas the linear construct displayed miR-7 sensitivity and was lowered by more than 40 ± 12% (mean ± s.e.m.) across biological replicates (Fig. 1d and Supplementary Fig. 4b), presumably owing to miRNA-mediated activation of deadenylation and subsequent exonucleolytic degradation. This suggests that the target sites in ciRS-7 do not support endocleavage by miR-7, and that ciRS-7 is resistant to the conventional miRNA destabilization of mRNA and therefore not prone to miR-7-dependent regulation.

To determine whether ciRS-7 serves as a binding platform for AGO2 and miR-7, we conducted Myc–AGO2 immunoprecipitation in HEK293 cells transiently co-expressing miR-7 or miR-769 as a control. By quantitative RT–PCR (qRT–PCR), endogenous ciRS-7

[1]Department of Molecular Biology and Genetics, Aarhus University, C.F. Møllers Alle 3, 8000C, Aarhus, Denmark. [2]Neurobiology Research, Institute of Molecular Medicine, University of Southern Denmark, J.B. Winsløwsvej 25, 5000C, Odense, Denmark. [3]Interdisciplinary Nanoscience Center (iNANO), Aarhus University, Gustav Wiedsvej 14, 8000C, Aarhus, Denmark.

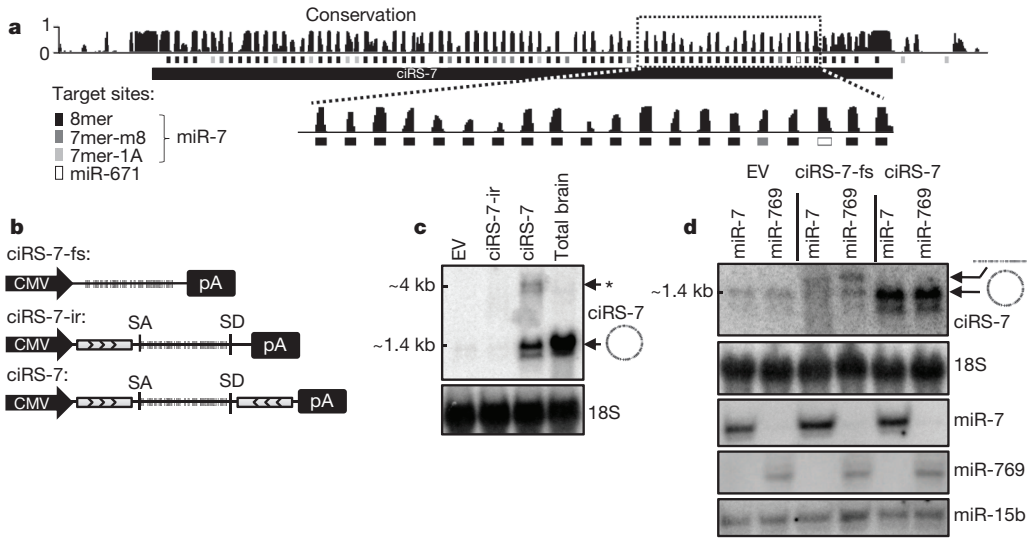

Figure 1 | Structure, conservation and heterologous expression of ciRS-7. **a**, Schematic representation of the genomic locus encoding human ciRS-7 and predicted miR-7 and miR-671 target sites are shown (grey-scaled according to target site strength). Mammalian conservation scores are depicted. The horizontal black bar represents the genomic location of ciRS-7. Magnification of a ciRS-7 sub-region is shown below. 8mer, 7mer-m8 and 7mer-1A targets denote conventional miRNA seed matches (specified in Supplementary Fig. 1a). **b**, ciRS-7 expression vectors are shown. ciRS-7-fs consists of the ciRS-7 exon without flanking sequences and splice sites; ciRS-7-ir includes splice sites and the endogenous flanking genomic sequence (1 kilobase (kb) upstream and 200 base pairs (bp) downstream). In ciRS-7, part of the upstream sequence has been inverted and inserted downstream, as illustrated by the directional bars. CMV, cytomegalovirus promoter; pA, polyadenylation signal; SA, splice acceptor; SD, splice donor. **c**, Northern blot with 5 μg of RNA from HEK293 cells transfected with empty vector (EV; pcDNA3), ciRS-7-ir (pcDNA3-ciR7-ir), ciRS-7 (pcDNA3-ciRS-7) or total RNA from human brain. The blot was probed against ciRS-7 and 18S ribosomal RNA (loading control). Migration of circular ciRS-7 and vector-based non-circular product (asterisk) are marked. **d**, Northern blot with 10 μg (agarose northern, top two panels) or 20 μg (PAGE northern, bottom three panels) of RNA from HEK293 cells co-transfected with empty vector, ciRS-7-fs or ciRS-7, together with miR-7 or miR-769 expression vectors (pJEBB-7 or pJEBB-769, respectively). The blots were hybridized with probes as indicated. 18S rRNA and miR-15b serve as loading controls.

pull-down by AGO2 was specifically enriched more than 50-fold in miR-7-transfected cells compared to miR-769-transfected cells (Fig. 2a), strongly suggesting that miR-7 is facilitating AGO association with ciRS-7. Furthermore, using a biotin-coupled miR-7 mimic, we observed a more than sixfold enrichment of ciRS-7 in the miR-7-captured fraction compared to the negative control, biotinylated miR-138 (Fig. 2b). To strengthen the observed formation of a ternary complex between miR-7, AGO2 and ciRS-7, we devised a T7 transcript containing all putative miR-7 target sites in conjunction with or without a streptavidin-aptamer motif[18] (Supplementary Fig. 5a, top). As expected, by incubating the linear T7 transcripts with lysate from HEK293 cells expressing either miR-7 or control miR-769, AGO2 and miR-7 were efficiently extracted only from miR-7-containing cell lysate and in an aptamer-specific fashion (Supplementary Fig. 5a–c). This demonstrates that the miR-7 sites within ciRS-7 are able to facilitate a specific miR-7–AGO2 interaction in cell lysates. Taken together, we conclude that the widespread AGO occupancy is caused by miR-7-directed association of AGO2 proteins to the prevalent and conserved miR-7 target sites in the ciRS-7 RNA.

To evaluate the subcellular localization of miR-7 and ciRS-7, we performed RNA- fluorescence *in situ* hybridization (FISH) in HEK293 (Fig. 2c, d) and HeLa (Supplementary Fig. 6a, b) cells co-transfected with ciRS-7 and miR-7. This showed a large degree of overlap between ciRS-7 and miR-7 within distinct cellular bodies, suggesting co-localization. Immunofluorescence co-staining with the P-body-specific marker DCP1A (ref. 19) revealed that ciRS-7 co-localized with P-bodies; however, this was only observed when the circRNA was co-expressed with miR-7, suggesting that miR-7 compartmentalizes ciRS-7 to the bodies (Fig. 2d and Supplementary Fig. 6b). Endogenous ciRS-7 and miR-7 signals also overlapped in primary cells isolated from mouse brain, as determined by dual fluorophore RNA-FISH analysis (Supplementary Fig. 6c).

To investigate whether miR-7 and ciRS-7 are globally co-expressed in the brain, we visualized their expression in the adult mouse brain using alkaline phosphatase-coupled miR-7 and ciRS-7 probes. The two RNAs showed a distinct neuronal expression (Fig. 2e) compared to mouse *Gapdh* mRNA (Supplementary Fig. 7a), comprising both cortical pyramidal neurons and interneurons (Fig. 2e; see legends to Fig. 2 and Supplementary Fig. 7 for further description of brain localization). At higher magnification, it was clear that ciRS-7 exhibited dendritic translocation (Supplementary Fig. 7b). Using confocal visualization of dual fluorophore RNA-FISH (Supplementary Fig. 7c) or 5-μm thin adjacent brain slides (Fig. 2e, bottom, and Supplementary Fig. 7d, e), miR-7 and ciRS-7 displayed clear co-expression in cells. The high expression of ciRS-7 coincides with miR-7 expression in mouse brain sections and in primary cells isolated from mouse brain, which strongly suggests that miR-7 is interacting endogenously with ciRS-7.

To test the effect of ciRS-7 expression on miR-7 activity, we constructed two luciferase reporters to monitor miR-7 activity by inserting either a perfect miR-7 target (Fig. 3a) or the entire ciRS-7 sequence (Fig. 3b) into the 3′-untranslated region (UTR) of *Renilla* luciferase. Co-transfecting the luciferase reporter with miR-7 and ciRS-7 expression vectors showed a substantial reduction of knockdown potential (ranging from two- to eightfold) when ciRS-7 was co-introduced with miR-7 (Fig. 3a, b). Comparably, the non-circRNA-producing vector ciRS-7-ir had little effect on knockdown; however, this may reflect low RNA production or inefficient circularization. Notably, the expression of ciRS-7 proved more efficient than a conventional anti-miRNA approach, suggesting that the ciRS-7 molecule is indeed a highly functional miRNA sponge. Similarly, using the 3′-UTR of human *EGFR*, which is a known target for miR-7, in a luciferase reporter assay, ciRS-7 reduced the knockdown efficiency exerted by miR-7 effectively (Supplementary Fig. 8a). Next, we evaluated the effect of ciRS-7 expression on miR-7-dependent regulation of endogenous targets. To this end, a single copy of the ciRS-7 expression vector was stably inserted into HeLa Flp-In cells that otherwise have no or very little endogenous expression of ciRS-7. Analysing the expression levels of the constructed HeLa cells by northern and qRT–PCR analysis revealed

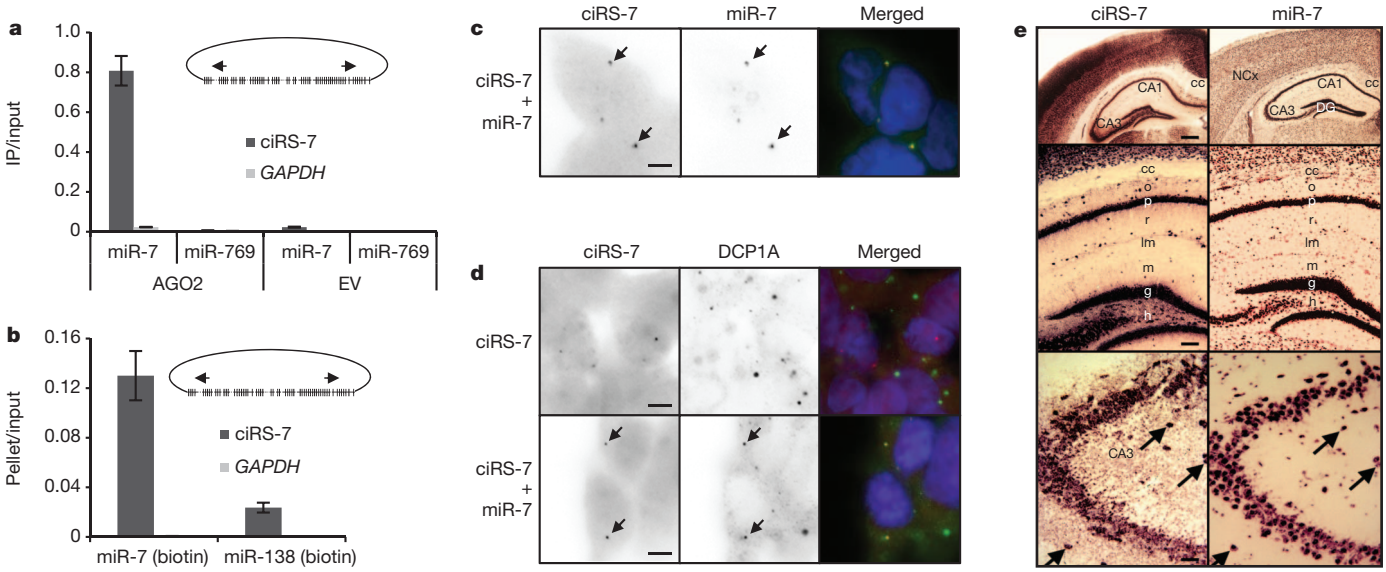

Figure 2 | Interaction between ciRS-7 and miR-7. a, Immunoprecipitation of Myc-tagged AGO2 from HEK293 cells transfected with either Myc–AGO2 plus pJEBB-7 (miR-7) or with Myc–AGO2 plus pJEBB-769 (miR-769). Empty vector serves as a Myc–AGO2 negative control. ciRS-7 and human *GAPDH* mRNA levels were quantified by qRT–PCR, and the relative immunoprecipitate (IP)/input ratios are plotted. Error bars represent s.d. ($n = 4$). **b**, The 3′-end biotinylated miRNA duplexes were transfected into HEK293 cells. After streptavidin capture, the input and bound fractions were evaluated by qRT–PCR (analysed as in **a**). **c**, RNA-FISH on HEK293 cells co-transfected with ciRS-7 (pcDNA3-ciRS-7) and miR-7 (pCK-7). ciRS-7 and miR-7 probes were labelled with Cy5 and Cy3, respectively. Scale bar, 5 μm. **d**, Combined immunofluorescence and RNA-FISH on ciRS-7-transfected HEK293 cells with or without miR-7 (pCK-7) co-transfection immunostained with human DCP1A antibody and hybridized with Cy5-labelled ciRS-7 probe. Scale bars, 5 μm. **e**, Mouse brains sections hybridized with probes specific for ciRS-7 (left) or miR-7 (right) showing intense neuronal expression throughout the neocortex (NCx), hippocampal subregions CA1 and CA3, and dentate gyrus (DG) (top and middle). Notably, miR-7 is also expressed in glial cells in the corpus callosum (cc, middle). Bottom panels show mouse brain *in situ* hybridization performed on apposing surfaces of 5-μm thin adjacent sections. Arrows point to large neurons that based on anatomical landmarks are present in both hybridizations. g, granule cell layer; h, dentate hilus; lm, stratum lacunosum-moleculare; m, stratum moleculare; o, stratum oriens CA1; p, pyramidal layer; r, stratum radiatum CA1. Scale bars, 200 μm (top), 100 μm (middle) and 50 μm (bottom).

ciRS-7 levels comparable to the endogenous levels observed in HEK293 cells, although still approximately 100-fold less than the total brain levels (Supplementary Fig. 9a).

As in HEK293 cells, the stably expressed ciRS-7 in HeLa cells was sensitive towards miR-671 as shown previously[8], but remained resistant to miR-7 (Supplementary Fig. 9b–d). Transfecting miR-7 in a dose-gradient manner revealed that established miR-7 targets (such as *SNCA*[20], *EGFR*[21] and *IRS2* (ref. 22)) responded more efficiently in the empty cell line without ciRS-7 expression (HeLa-EV) compared to ciRS-7-expressing cells (HeLa-ciRS-7) (Fig. 3c–e). In addition, when transfecting miR-671 into HeLa-ciRS-7 before introducing dose-gradient miR-7 levels, the evaluated target genes significantly regained

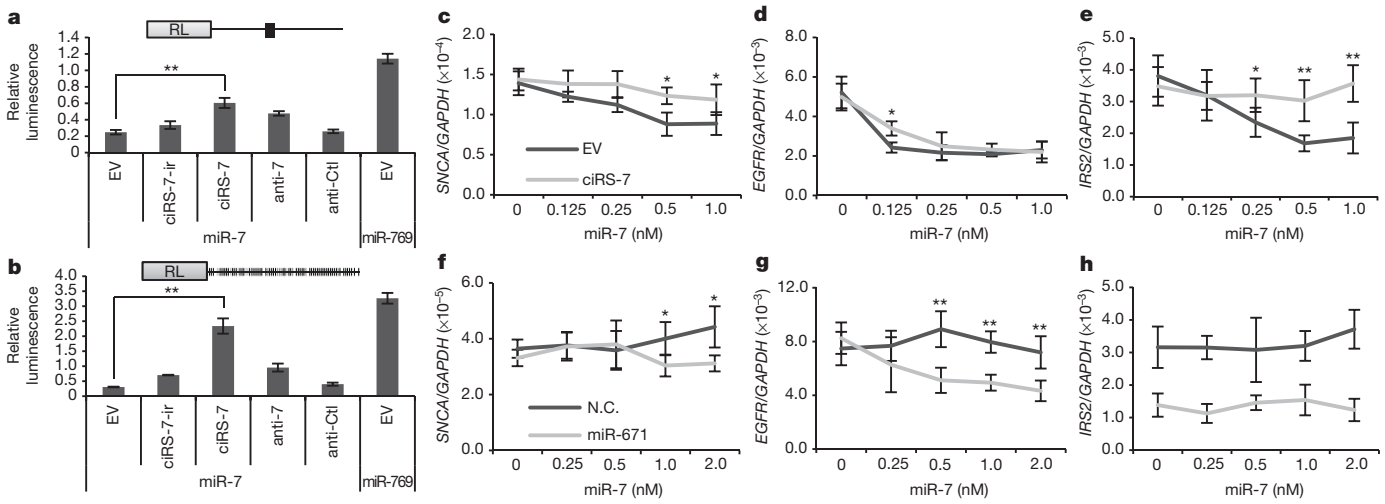

Figure 3 | ciRS-7 acts as a sponge for miR-7 activity. a, **b**, Luciferase reporter assays using reporter constructs with either a perfect miR-7 target site (**a**) or the entire ciRS-7 sequence (**b**). HEK293 cells in 12-well dishes were transfected with 0.5 μg empty vector (pcDNA3), ciRS-7-ir (pcDNA3-ciR7-ir), ciRS-7 (pcDNA3-ciRS-7), 50 nM anti-miR-7 (anti-7) or 50 nM anti-miRNA control (anti-Ctl), together with 0.2 μg miR-7 (pJEBB-7) or miR-769 (pJEBB-769) and 0.1 μg psiCheck reporter. The relative levels of *Renilla* luminescence (RL) normalized to firefly luminescence are plotted. Error bars represent s.d. ($n = 3$). **c**–**e**, qRT–PCR analysis of human *SNCA* mRNA (**c**), *EGFR* mRNA (**d**) and *IRS2* mRNA (**e**) levels in HeLa-ciRS-7 (light grey line) or HeLa-EV cells (dark grey line) transfected with increasing concentrations of miR-7 as indicated. **f**–**h**, qRT–PCR analysis of human *SNCA* (**f**), *EGFR* (**g**) and *IRS2* (**h**) mRNA levels in HeLa-ciRS-7 cells transfected with miR-671 mimic short interfering RNA (miR-671; light grey line) or negative control (N.C.; dark grey line) siRNA 24 h before transfection with increasing concentrations of miR-7. Error bars represent s.d. ($n = 4$). *$P < 0.05$; **$P < 0.01$.

miR-7 sensitivity compared to control transfections (Fig. 3f–h). This suggests that miR-671 probably functions as an indirect regulator of miR-7 activity by targeting and reducing ciRS-7 levels. In line with this, the sponge effect correlates with ciRS-7 expression levels (Supplementary Fig. 8b), which after extrapolation indicates that the much higher expression of ciRS-7 in the brain exerts a stronger sponge efficiency here compared to the effect shown in HeLa-ciRS-7.

The existence of a circRNA acting as a potent miRNA sponge immediately raises the question whether circular miRNA sponges are a more general phenomenon. Indeed, by predicting miRNA target sites in the other well-known circular, testis-specific *Sry* RNA, we identified 16 putative target sites for miR-138 (Fig. 4a). To study a direct interaction between miR-138 and *Sry*, we devised a vector expressing *Sry* circRNA (Supplementary Fig. 10a). Biogenesis of circular *Sry* was verified by northern blotting and RT–PCR (Supplementary Fig. 10b, c). To validate that *Sry* circRNA can act as a miR-138 sponge, we inserted the *Sry* sequence into a luciferase reporter construct and tested the knockdown potential of miR-138 in the presence or absence of circular *Sry* RNA. Indeed, after co-expression of miR-138, we observed a fourfold reduction of relative luminescence compared to miR-769 expression, suggesting that the miR-138 target sites facilitate a miRNA effect (Fig. 4b). By co-expression of circular *Sry* RNA, the knockdown potential of miR-138 was significantly diminished (Fig. 4b), however, presumably owing to modest circular RNA biogenesis from the *Sry* expression vector (10- to 20-fold below ciRS-7, data not shown), the sponge effect here was less pronounced. Immunoprecipitation of Myc-tagged AGO2 from miR-138-transfected cells resulted in a more than tenfold enrichment of *Sry* circRNA compared to miR-769-transfected cells (Fig. 4c). Furthermore, using biotin-labelled miR-138, *Sry* circRNA was specifically captured (sixfold enrichment compared to biotin-labelled miR-7; Fig. 4d), suggesting that *Sry* circRNA is able to interact with miR-138. Thus, we propose that the circular *Sry* RNA functions as a miR-138 sponge.

Recently, circRNA was found to be a highly prevalent RNA species in the human transcriptome[23]. Our observation that very abundant endogenous circRNA molecules, which are inherently resistant to exonucleolytic RNA decay, can serve as efficient miRNA sponges, adds to the growing repertoire of regulatory functions in gene expression. Considering the widespread involvement of miR-7 as a key regulator of various cancer pathways[21,24] and the suggested implication of miR-7 in Parkinson's disease by direct targeting of α-synuclein protein expression[20], ciRS-7 probably serves as a crucial factor significantly engaged in the functioning of neurons as well as a responsible candidate in neurological disorders and brain tumour development.

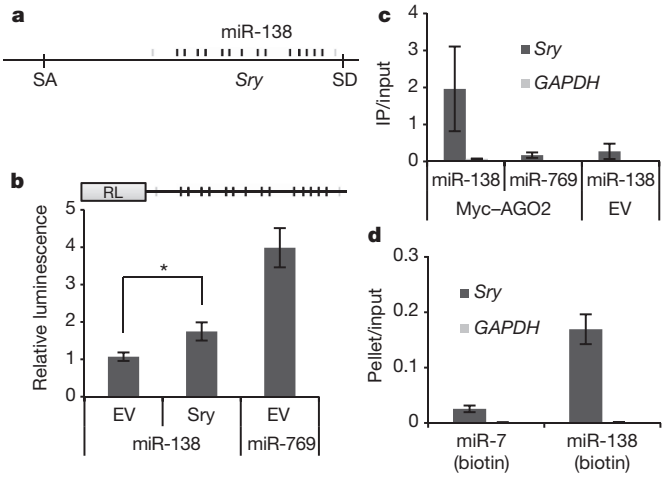

Figure 4 | Circular *Sry* RNA interacts with miR-138. **a**, Diagram of the mouse *Sry* locus indicating splice acceptor and splice donor sites facilitating *Sry* circularization. Perpendicular lines represent putative target sites for miR-138 (target site code as in Fig. 1a). **b**, Luciferase reporter assays with the entire *Sry* sequence. Luminescence was measured 48 h after transfection with the luciferase reporter (psiCheck-Sry) and expression vectors for miR-138 (pJEBB-138) or miR-769 (pJEBB-769) and with empty vector (pcDNA3; EV) or *Sry* expression vector (pcDNA3-Sry). The relative levels of *Renilla* luminescence normalized to firefly luminescence are plotted. Error bars represent s.d. ($n = 3$). *$P < 0.05$. **c**, Immunoprecipitation of Myc-tagged AGO2 from HEK293 cells co-transfected with the *Sry* expression vector, Myc–AGO2 or empty vector and pJEBB-138 or pJEBB-769 as noted. Mouse *Sry* circRNA and human *GAPDH* levels were quantified by qRT–PCR and the relative immunoprecipitate/input ratios are plotted. Error bars represent s.d. ($n = 4$). **d**, As described in Fig. 2b, 3′-biotinylated miR-7 or miR-138 was transfected into HEK293 cells along with the *Sry* expression vector. *Sry* circRNA and *GAPDH* levels were analysed in the input and bound fractions by qRT–PCR. Error bars represent s.d. ($n = 4$).

METHODS SUMMARY

Transfections were conducted using calcium phosphate procedure or Lipofectamine 2000 (Invitrogen). RNA was isolated using TRIzol (Invitrogen) according to manufacturer's protocol. Northern blotting was conducted on 1.2% agarose or 12% PAGE, transferred to Hybond-N^+ membranes (GE Healthcare) and hybridized in Church buffer (see Methods). AGO immunoprecipitation was conducted as described previously[25]. Biotin-labelled miRNAs were transfected into HEK293 cells at a final concentration of 20 nM and treated similar to AGO immunoprecipitation. FISH was performed on paraformaldehyde-fixed cells transfected with constructs as indicated, and treated as described in Methods. Mouse brain sections (30 or 5 μm) were made from 8–9-week-old C57BL/6 male mice. Subsequent *in situ* hybridization was performed using custom-designed alkaline phosphatase-labelled DNA and LNA probes. Luciferase assays were performed with the dual-luciferase reporter assay kit (Promega). Reverse transcription and quantitative PCR were conducted using MLV-RT (Invitrogen) and Platinum SYBR Green qPCR Supermix UDG (Invitrogen), respectively.

Full Methods and any associated references are available in the online version of the paper.

Received 16 August 2012; accepted 8 February 2013.
Published online 27 February 2013.

1. Bartel, D. P. MicroRNAs: target recognition and regulatory functions. *Cell* **136,** 215–233 (2009).
2. Franco-Zorrilla, J. M. *et al.* Target mimicry provides a new mechanism for regulation of microRNA activity. *Nature Genet.* **39,** 1033–1037 (2007).
3. Poliseno, L. *et al.* A coding-independent function of gene and pseudogene mRNAs regulates tumour biology. *Nature* **465,** 1033–1038 (2010).
4. Cesana, M. *et al.* A long noncoding RNA controls muscle differentiation by functioning as a competing endogenous RNA. *Cell* **147,** 358–369 (2011).
5. Karreth, F. A. *et al. In vivo* identification of tumor-suppressive PTEN ceRNAs in an oncogenic BRAF-induced mouse model of melanoma. *Cell* **147,** 382–395 (2011).
6. Tay, Y. *et al.* Coding-independent regulation of the tumor suppressor PTEN by competing endogenous mRNAs. *Cell* **147,** 344–357 (2011).
7. Sumazin, P. *et al.* An extensive microRNA-mediated network of RNA–RNA interactions regulates established oncogenic pathways in glioblastoma. *Cell* **147,** 370–381 (2011).
8. Hansen, T. B. *et al.* miRNA-dependent gene silencing involving Ago2-mediated cleavage of a circular antisense RNA. *EMBO J.* **30,** 4414–4422 (2011).
9. Capel, B. *et al.* Circular transcripts of the testis-determining gene *Sry* in adult mouse testis. *Cell* **73,** 1019–1030 (1993).
10. Ebert, M. S., Neilson, J. R. & Sharp, P. A. MicroRNA sponges: competitive inhibitors of small RNAs in mammalian cells. *Nature Methods* **4,** 721–726 (2007).
11. Bailey, T. L. & Elkan, C. Fitting a mixture model by expectation maximization to discover motifs in biopolymers. *Proc. Int. Conf. Intell. Syst. Mol. Biol.* **2,** 28–36 (1994).
12. Elbashir, S. M., Martinez, J., Patkaniowska, A., Lendeckel, W. & Tuschl, T. Functional anatomy of siRNAs for mediating efficient RNAi in *Drosophila melanogaster* embryo lysate. *EMBO J.* **20,** 6877–6888 (2001).
13. Hutvágner, G. & Zamore, P. D. A microRNA in a multiple-turnover RNAi enzyme complex. *Science* **297,** 2056–2060 (2002).
14. Chi, S. W., Zang, J. B., Mele, A. & Darnell, R. B. Argonaute HITS-CLIP decodes microRNA–mRNA interaction maps. *Nature* **460,** 479–486 (2009).
15. Bak, M. *et al.* MicroRNA expression in the adult mouse central nervous system. *RNA* **14,** 432–444 (2008).
16. Pasman, Z., Been, M. D. & Garcia-Blanco, M. A. Exon circularization in mammalian nuclear extracts. *RNA* **2,** 603–610 (1996).
17. Dubin, R. A., Kazmi, M. A. & Ostrer, H. Inverted repeats are necessary for circularization of the mouse testis *Sry* transcript. *Gene* **167,** 245–248 (1995).
18. Iioka, H., Loiselle, D., Haystead, T. A. & Macara, I. G. Efficient detection of RNA-protein interactions using tethered RNAs. *Nucleic Acids Res.* **39,** e53 (2011).

19. Liu, J., Valencia-Sanchez, M. A., Hannon, G. J. & Parker, R. MicroRNA-dependent localization of targeted mRNAs to mammalian P-bodies. *Nature Cell Biol.* **7,** 719–723 (2005).
20. Junn, E. *et al.* Repression of α-synuclein expression and toxicity by microRNA-7. *Proc. Natl Acad. Sci. USA* **106,** 13052–13057 (2009).
21. Kefas, B. *et al.* microRNA-7 inhibits the epidermal growth factor receptor and the Akt pathway and is down-regulated in glioblastoma. *Cancer Res.* **68,** 3566–3572 (2008).
22. Jiang, L. *et al.* MicroRNA-7 targets IGF1R (insulin-like growth factor 1 receptor) in tongue squamous cell carcinoma cells. *Biochem. J.* **432,** 199–205 (2010).
23. Salzman, J., Gawad, C., Wang, P. L., Lacayo, N. & Brown, P. O. Circular RNAs are the predominant transcript isoform from hundreds of human genes in diverse cell types. *PLoS ONE* **7,** e30733 (2012).
24. Reddy, S. D., Ohshiro, K., Rayala, S. K. & Kumar, R. MicroRNA-7, a homeobox D10 target, inhibits p21-activated kinase 1 and regulates its functions. *Cancer Res.* **68,** 8195–8200 (2008).
25. Hendrickson, D. G., Hogan, D. J., Herschlag, D., Ferrell, J. E. & Brown, P. O. Systematic identification of mRNAs recruited to Argonaute 2 by specific microRNAs and corresponding changes in transcript abundance. *PLoS ONE* **3,** e2126 (2008).

Supplementary Information is available in the online version of the paper.

Acknowledgements We thank C. Bus and R. Rosendahl for technical assistance and R. M. Zadegan for art work. We also thank the G. Hannon laboratory for providing us with the Myc-tagged AGO2 expression vector, J. Lykke-Andersen for the DCP1A antibody, and K. L. Lambertsen and C. U. von Linstow for their assistance with confocal microscopy. This work was supported by the SIROCCO EU consortium, the Lundbeck Foundation, and the Danish Council for Independent Research - Natural Sciences. T.B.H. and B.H.C. were supported by the Lundbeck Foundation.

Author Contributions T.B.H. conceived the project, designed the experiments and drafted the manuscript. T.B.H., T.I.J. and C.K.D. performed the experiments. J.B.B. assisted experimentally and intellectually. B.H.C. performed the brain *in situ* hybridizations. B.F., C.K.D. and J.K. supervised the project and revised the manuscript.

Author Information Reprints and permissions information is available at www.nature.com/reprints. The authors declare no competing financial interests. Readers are welcome to comment on the online version of the paper. Correspondence and requests for materials should be addressed to J.K. (jk@mb.au.dk) or T.B.H. (tbh@mb.au.dk)

METHODS

Constructs and transfections. HEK293 Flp-In T-Rex (Invitrogen) and HeLa Flp-In (Invitrogen) cells were maintained under standard culture conditions. Transfections were conducted with either calcium phosphate using standard procedures or Lipofectamine 2000 (Invitrogen) according to supplier's protocol. The construction of pJEBB-769 has been published previously[8]. pJEBB-7 and pJEBB-138 were constructed similarly; PCR amplification of the miR-7-1 locus was performed using miR-7 forward/reverse primers, or the miR-138 locus (in mouse) using miR-138 forward/reverse primers, and the fragments were inserted into a NotI- and SalI-digested enhanced green fluorescent protein (eGFP) expression cassette (pJEBB). pCK-7 was generated by digesting pJEBB-7 with NotI and XbaI and inserting the resulting fragment into NotI- and XbaI-digested pCK.

pcDNA3-ciRS-7-ir was constructed by PCR amplifying the circRNA locus, including 1 kb upstream and 200 bp downstream to the nonlinear splice sites, using ciRS-7 forward/reverse primers. The PCR fragment was inserted into HindIII- and NotI-digested pcDNA3 (Invitrogen). An ~800-bp DNA stretch upstream of the splice acceptor was amplified using ciRS-7-ir forward/reverse primers and inserted downstream in the reverse orientation in an XhoI-digested pcDNA3-ciRS-7-ir, thus generating pcDNA3-ciRS-7. For the generation of pcDNA3-ciRS-fs, PCR amplification of the ciRS-7 exon using ciRS-7-fs forward/reverse primers was inserted into pcDNA3 using HindIII and XhoI. To establish HeLa cells stably expressing ciRS-7, ciRS-7 was copy-pasted into pcDNA5 using HindIII and ApaI, and transfected into HeLa Flp-In cells (Invitrogen) along with pOG44. Forty-eight hours after transfections, the cell media was supplemented with hygromycin B according to manufacturer's protocol.

pcDNA3-Sry was constructed by PCR amplifying the *Sry* locus from male mouse DNA using Sry forward/reverse primers, and inserting the amplicon into pcDNA3 using BamHI and NotI. Subsequently, SalI-digested CMV promoter from pcDNA5 was inserted into the XhoI site in an inverse orientation.

Luciferase reporter vectors were constructed by inserting annealed primers (miR-7-psiCheck forward/reverse) or PCR amplicons (produced by ciRS-7-psiCheck forward/reverse, Sry-psiCheck forward/reverse or EGFR-psiCheck forward/reverse) into the psiCheck-2 vector.

Transfection of miRNA mimics (miR-7-5p and miR-671-5p, Applied Biosystems) was conducted using Lipofectamine 2000 (Invitrogen). In case of dose-gradient transfections, a total concentration of 10 nM was used with varying ratios between miR-7 and negative control oligonucleotide, as indicated.

Northern blotting. For miRNA, 20–30 μg whole cell RNA was loaded on a 12% denaturing PAGE gel. RNA was transferred to Amersham hybond-N+ membranes (GE Healthcare). The membranes were hybridized with [^{32}P]-labelled DNA oligonucleotides (listed in Supplementary Table 1) in Church buffer (0.5 M $NaPO_4$, 7% SDS, 1 mM EDTA, 1% BSA, pH 7.5) at 37 °C and washed in 2× SSC (300 mM NaCl, 30 mM Na-citrate, pH 7.0) with 0.1% SDS at room temperature. The membranes were exposed on phosphorimager screens and analysed using Quantity One or Image Lab software (Bio Rad).

For circRNA, agarose northern blot was performed with 5–10 μg RNA separated in 1.2% agarose. Subsequent hybridization and wash was carried out at 55 °C and 50 °C, respectively, otherwise conducted as described above.

AGO immunoprecipitation. Myc-tagged AGO2 was co-transfected with either pJEBB-7 or pJEBB-769 in p10 dishes. Forty-eight hours after transfection, AGO immunoprecipitation was performed as described previously[25]. In brief, cells were lysed in 150 mM KCl, 25 mM Tris-HCl, pH 7.4, 5 mM EDTA, 0.5% Triton X-100 and 5 mM dithiothreitol (DTT) supplemented with Ribolock (Fermentas) and proteinase inhibitor cocktail (Roche). The lysate was mixed with Myc antibody (Abcam, ab9106) coupled sepharose beads (GE Healthcare) and left under rotation for 4 h at 4 °C. Beads were subsequently washed five times in lysis buffer and the RNA was extracted using TRIzol reagent (Invitrogen).

Streptavidin aptamer. T7 transcription was performed on PCR products containing the entire circRNA sequence with or without the inclusion of a streptavidin aptamer sequence using T7 MEGAscript (Ambion). The streptavidin-based capturing of RNA with associated proteins was conducted as previously published[18]. In brief, the T7 transcript was renatured and mixed with streptavidin beads (Dynabeads MyOne Streptavidin C1, Invitrogen) for 1 h at 4 °C and washed twice in lysis buffer (10 mM HEPES, pH 7.0, 200 mM NaCl, 1% Triton X-100, 10 mM $MgCl_2$ and 1 mM DTT). Cells transfected 48 h before collection with either pJEBB-7 or pJEBB-769 were lysed and added to the RNA-coupled beads using half a confluent p10 dish per streptavidin capture. After rotating for 4 h at 4 °C, the beads were washed five times and RNA and protein were extracted and analysed by northern blot (probes listed in Supplementary Table 1) and by western blot using anti-AGO2 (Abcam, ab57113) and anti-HuR (Santa Cruz, SC-5261) as a loading control.

Biotin-coupled miRNA capture. Biotin-labelled miRNAs were transfected into HEK293 cells at a final concentration of 20 nM. Forty-eight hours after transfection, cells were collected and treated as described above.

Immunofluorescence and RNA-FISH. Cells were seeded on glass coverslips in 12-well plates and transfected with ciRS-7 and pCK-7 using calcium phosphate (HEK293 cells) or Lipofectamine 2000 (HeLa cells). Forty-eight hours after transfection, cells were washed in PBS and fixed in 4% paraformaldehyde for 15 min and permeabilized overnight in 70% ethanol. Cells were then washed twice in PBS containing 5 mM $MgCl_2$ (PBSM), and rehydrated for 10 min in 50% formamide and 2× SSC. In case of immunofluorescence, cells were blocked with 3% BSA in PBSM for 1 h followed by incubation with primary antibody (human DCP1A (ref. 26)) in 3%BSA/PBSM supplemented with RNaseOUT (Fermentas) at 37 °C. After washing three times in PBSM, cells were incubated with secondary antibody (Alexa Fluor 488, A21206, Invitrogen). Cells were then washed three times before proceeding with RNA-FISH.

For FISH, cells were incubated at 37 °C in a solution containing 50% formamide, 2× SSC, 0.25 mg ml^{-1} *Escherichia coli* transfer RNA, 0.25 mg ml^{-1} salmon sperm DNA (Invitrogen), 2.5 mg ml^{-1} BSA (Roche), and 0.5 ng ml^{-1} fluorescently labelled ciRS-7 (Supplementary Table 1) and miR-7 (Exiqon) probes. After 3 h, cells were washed twice for 20 min at 37 °C in 50% formamide and 2× SSC, followed by four 5-min washes in PBS (the penultimate wash containing 4′,6-diamidino-2-phenylindole (DAPI)) and an additional brief wash in nuclease-free water. Cells were mounted in ProLong Gold (Invitrogen) and left overnight at room temperature.

Mice for the *in vivo* study. This study was performed in accordance with guidelines approved by the Danish Animal Ethical Committee (no. 2011/561-1950), using 8–9-week-old C57BL/6 male mice ($n = 5$) (Taconic). The mice were euthanized by cervical dislocation, the brains frozen in gaseous CO_2 and processed into 30-μm or 5-μm coronal cryostat sections. For paraformaldehyde-fixed tissue, brains were fixed and processed into 16-μm sections for histological analysis as described previously[27].

***In situ* hybridization.** *In situ* hybridization was performed as previously described[28] using custom designed alkaline phosphatase-labelled DNA and LNA probes (Supplementary Table 1) recognizing mouse *Gapdh*, ciRS-7 and miR-7 (DNA Technology A/S). Double fluorescence *in situ* hybridization was performed on fixed tissue. Sections were rinsed for 10 min in TBS buffer containing 0.5% Triton X-100 (ref. 27) and incubated overnight with Maxima Probe/master mix (Thermo Scientific) containing Cy3-labelled ciRS-7 and Cy5-labelled miR-7 probes. Development was arrested by rinsing the sections at 37 °C in tap water and distilled water, before mounting with Aquatex (Merck). The specificity of the signal was tested by hybridizing parallel sections with: (1) 100-fold excess of unlabelled probe, (2) pre-treatment with RNase A (Pharmacia Biotech), (3) buffer alone, or (4) Cy5-labelled miR-449 probe. All controls were devoid of signal.

Estimation of the percentage of ciRS-7- and miR-7-co-expressing neurons was performed in layer IV–V of the cingulate gyrus. ciRS-7- and miR-7-expressing neurons were counted on digitalized images of pairs of adjacent 5-μm thick sections. Per section, 75 randomly selected ciRS-7-expressing neurons were counted and analysed for co-expression of miR-7. Only ciRS-7-expressing neurons with a clearly identifiable nucleus were analysed. For control, a comparable number of circular regions devoid of ciRS-7 was analysed for miR-7 expression.

Luciferase reporter assay. HEK293 cells seeded in 12-well plates and collected 48 h after transfection using the dual-luciferase reporter assay kit (Promega). In case of anti-miRNA experiments, anti-miRNA inhibitor (Applied Biosystems) was used at a final concentration of 50 nM. Luminescence was measured on a BMG FLUOstar luminometer (BMG labtech).

Tobacco acid pyrophosphatase exonuclease and RNase R treatment. In case of tobacco acid pyrophosphatase exonuclease, 4 μg of RNA was incubated with 10 U of tobacco acid pyrophosphatase (Epicentre) at 37 °C for 1 h. After incubation, the RNA was ethanol precipitated and incubated with 1 U of Terminator 5′-dependent exonuclease (Epicentre). In case of RNase R, 4 μg of RNA was incubated with 20 U of RNase R (Epicentre) at 30 °C for 10 min. In both cases, half the RNA was visualized by northern blotting, the other half was subjected to qRT–PCR as described below.

qRT–PCR. Total RNA was extracted from cells in culture using TRIzol reagent (Invitrogen) according to standard procedures. Complementary DNA for qRT–PCR expression analyses was synthesized from total RNA by MLV-RT (Invitrogen) according to the supplied protocol using random hexamer primer. Quantitative PCR was performed with Platinum SYBR Green qPCR Supermix UDG (Invitrogen) on either MxPro3000 cycler (Stratagene) or LightCycler 480 (Roche) according to standard procedures, using primers listed in Supplementary

Table 1. RNA levels were normalized to human *GAPDH*. In case of miRNA Taqman qPCR, miR-7, miR-769 and RNU48 assays (Applied Biosystems) were used adhering to manufacturer's protocol. All quantitative PCR reactions were conducted in quadruplicates.

In case of 3′-rapid amplification of cDNA ends (RACE), cDNA synthesis was primed by oligo-dTN. PCR was subsequently conducted using the 3′-RACE reverse/ciRS-7 (2) forward primer set.

Statistical analysis. Statistical significance was determined by the standard two-tailed Student's *t*-test.

26. Lykke-Andersen, J. & Wagner, E. Recruitment and activation of mRNA decay enzymes by two ARE-mediated decay activation domains in the proteins TTP and BRF-1. *Genes Dev.* **19,** 351–361 (2005).
27. Clausen, B. H. *et al.* Interleukin-1β and tumor necrosis factor-α are expressed by different subsets of microglia and macrophages after ischemic stroke in mice. *J. Neuroinflammation* **5,** 46 (2008).
28. Clausen, B. H., Lambertsen, K. L. & Finsen, B. Glyceraldehyde-3-phosphate dehydrogenase versus toluidine blue as a marker for infarct volume estimation following permanent middle cerebral artery occlusion in mice. *Exp. Brain Res.* **175,** 60–67 (2006).